

## Antibacterial Activity of Undoped and Cu<sup>2+</sup> Doped Tin Oxide Nanoparticles Synthesized by Microwave Irradiated Solvothermal Method

K.J. ABHIRAMA<sup>1,\*</sup>, N.SARASWATHI<sup>2</sup> and K.U. MADHU<sup>3</sup>

<sup>1</sup>Department of Physics, Sree Devi Kumari Women's College, Kuzhithurai-629163, India

<sup>2</sup>Department of Physics, Arignar Anna College, Aralvaimozhi-629301, India

<sup>3</sup>Department of Physics, S.T. Hindu College, Nagercoil-629002, India

\*Corresponding author: E-mail: abhiramathampi87@gmail.com

Received: 18 January 2022;

Accepted: 6 April 2022;

Published online: 15 June 2022;

AJC-20853

In present work, a simple and facile microwave irradiated solvothermal method was applied for the synthesis of undoped and Cu<sup>2+</sup> doped tin oxide nanoparticles. Thermal characterization was performed to study the thermal stability and to fix the annealing temperature. All the prepared samples were annealed at 500 °C and then characterized. Structural, morphological and optical characterizations were done using PXRD, TEM, SEM and UV-Vis NIR analysis. The PXRD measurement shows the tetragonal phase of tin oxide. Agglomerated and spherical morphology was observed in SEM and TEM micrographs. Presence of blue shift was observed in the absorption spectra of the prepared samples. Elemental compositions of the samples were analyzed using EDX patterns. Magnetic characterization was performed using vibrating sample magnetometer and the analysis revealed that the prepared samples were diamagnetic in nature. Antibacterial studies showed the efficient activity against the Gram-positive and Gram-negative bacterial stains.

**Keywords:** Solvothermal, Agglomeration, Annealing, Elemental composition, Antibacterial activity.

### INTRODUCTION

In past decades, nanostructured materials has evolved as a separate class due to its unique properties and its importance. Nanoscience is the study of phenomena and manipulation of materials at atomic and molecular scales. The physical and chemical properties of nanostructured materials are different from that of bulk materials even though they have same chemical composition. Nanostructured materials form a bridge between the molecules and the bulk materials [1]. In the field of technology metal oxide nanostructured materials possess considerable interest due to their wide applications [2]. The quantum confinement and quantization of conduction electrons by small volume of nanocrystals enhances the optical and electrical conductance and it makes the metal nanoparticles a fascinating area of research. Metal clusters can exhibit attractive electronic properties when the crystallite size reaches the order of de Broglie wavelength of conduction electrons [3].

SnO<sub>2</sub> is n-type semiconductor material with a wide band gap of 3.6-3.8 eV [4] and has a tetragonal structure. Tin oxide

is abundant chemically stable and has high electrical conductivity. SnO<sub>2</sub> nanoparticles can be used as catalyst for the removal of dyes [5,6], as gas sensors [7,8], as anodes in lithium ion batteries [9,10], etc. Synthetic techniques such as sol gel method [11], solvothermal method [12], spray pyrolysis [13], hydrothermal [14], pulsed laser deposition [15], precipitation method [16], wet chemical method [17] and microwave assisted method [18] were adopted by researchers for the synthesis of tin oxide nanoparticles. Zhang *et al.* [19] adopted the spark plasma technique for the preparation of antimony doped tin oxide nanoceramics. High ball mill mechanochemical processing was followed by Sabri *et al.* [20] to synthesize Mn doped SnO<sub>2</sub> nanoparticles.

Microbiological contaminants such as bacteria and viruses are considered as colloids having particle size in micrometer and nanometer range [21]. Nanomaterials may interact with biomolecules and cellular process [22]. Improper and wide spread use of antibiotics in various fields had led to the development of antibiotic resistant microbial strain [23]. Common bacterial species such as *Staphylococcus aureus*, *Escherichia*

*coli* are resistant to antibiotics and this lead to a serious issue among mankind. Metal oxide nanoparticles are considered as the effective one for the treatment of infectious diseases to that of antibiotic-resistant bacteria [24]. Antibacterial activity of metal oxide nanoparticles such as SnO<sub>2</sub>, ZnO, CuO, Fe<sub>2</sub>O<sub>3</sub> against various test stains was reported [25-27]. In present work, a simple and cost effective microwave assisted solvothermal technique is adopted using a simple domestic microwave oven for the synthesis of undoped and Cu<sup>2+</sup> doped SnO<sub>2</sub> nanoparticles. The prepared samples were annealed at 500 °C and then characterized.

## EXPERIMENTAL

All the reagents and solvents required for the synthesis of SnO<sub>2</sub> nanoparticles were commercially available and used as received.

**Synthesis of SnO<sub>2</sub> nanoparticles:** Stannous chloride dihydrate, urea, ethylene glycol and copper acetate were used as precursors for the synthesis of undoped and Cu<sup>2+</sup> doped SnO<sub>2</sub> nanoparticles. To prepare SnO<sub>2</sub> sample stannous chloride dihydrate and urea were taken in the molecular ratio 1:3 and dissolved separately in 200 ml ethylene glycol (solvent). Urea solution was added dropwise into stannous chloride solution kept under stirring in a magnetic stirrer. The Cu<sup>2+</sup> doped SnO<sub>2</sub> samples were prepared by taking 1 mol% Cu(CH<sub>3</sub>COO)<sub>2</sub> with the above precursors used for the preparation of undoped samples. The dissolved solution was kept in a domestic microwave oven (Onida model-Power Solo 20) operated with a frequency of 2.45 GHz and power 800 Watts). Microwave irradiation was continued till the solvent evaporates and form a colloidal precipitate. The precipitate was washed with double distilled water for about six times to remove the water soluble impurities and then about three times with acetone to remove the organic impurities present. The washed samples were dried in atmospheric air and preserved as yield.

**Characterization:** The TGA and DTA analysis were carried out for undoped SnO<sub>2</sub> nanoparticles with NETZSCH STA 409 C/CD. Then the prepared samples were annealed at 500 °C for about 1 h. The annealed samples were characterized by powder X-ray diffraction analysis using X'Pert Pro-Panalytic instrument to analyze the structure of the prepared sample. SEM and TEM analysis was carried out to recognize the morphology. Elemental compositions of the samples were identified using EDX patterns. The optical band gap energy was calculated using UV-visible spectrophotometer Cary 5000 model instrument. The magnetic measurements were carried out using Lakeshore, USA, model 7407 Vibrating Sample Magnetometer.

**Antibacterial activity:** The antibacterial activity of the prepared samples was carried out using Agar disc diffusion method with *Staphylococcus aureus* and *Escherichia coli* as the test stains.

## RESULTS AND DISCUSSION

**TG/DTA studies:** To improve the phase purity, ordering of the samples and to choose the appropriate annealing temperature thermal analysis was performed using TGA and DTA

analysis under nitrogen atmosphere in the temperature range 30-800 °C. The TG/DTA analysis pattern is shown in Fig. 1. Below 100 °C, a sharp decrease in the TG curve was observed, which was mainly due to the evaporation of water adsorbed on the particle surface [28]. Occurrence of exothermic peak around 307 °C was observed in the DTA curve and it was due to the decomposition of organic residues and tin oxide nanoparticles formation [29]. Around 300 °C, the TG curve shows a slight increase in weight and it may be due to oxidation of SnO to form SnO<sub>2</sub>. As temperature increases no such increase in weight was observed and the sample attains thermal stability around 800 °C. In this work, the annealing temperature was fixed as 500 °C and annealed all the samples at this temperature for about 1 h and then used to carry out further characterization.

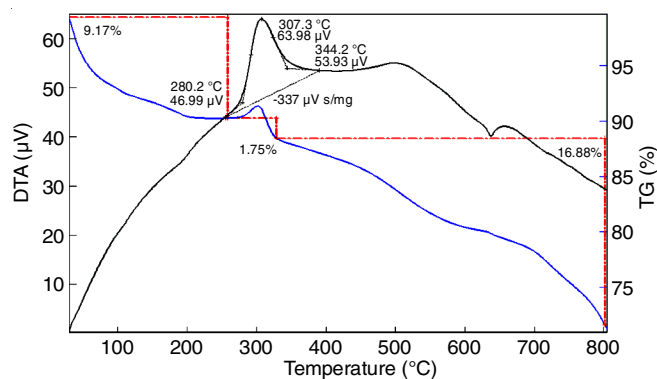


Fig. 1. TG/DTA curves for SnO<sub>2</sub> nanoparticles

**PXRD studies:** The PXRD patterns of undoped and Cu<sup>2+</sup> doped SnO<sub>2</sub> nanoparticles are shown in Fig. 2. The peaks in the PXRD pattern of SnO<sub>2</sub> and Cu<sup>2+</sup> doped SnO<sub>2</sub> matches well with the tetragonal phase of tin dioxide (JCPDS card no.: 88-0287). The cell parameter values of standard and prepared SnO<sub>2</sub> are tabulated in Table-1.

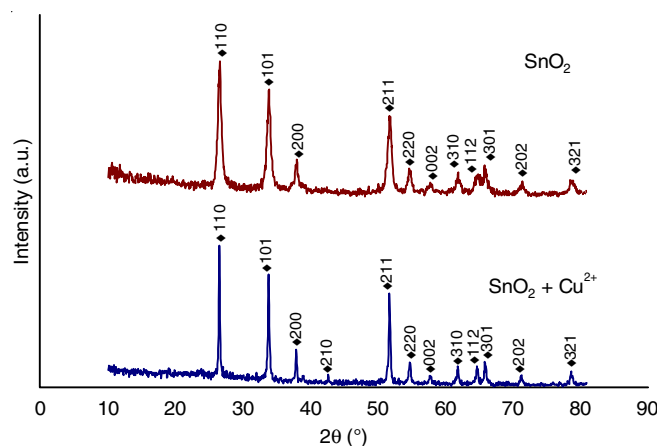


Fig. 2. PXRD pattern of undoped and Cu<sup>2+</sup> doped SnO<sub>2</sub> nanoparticles

TABLE-1  
CELL PARAMETER VALUES OF SnO<sub>2</sub>

| System                              | Standard value |       | Calculated value |        |
|-------------------------------------|----------------|-------|------------------|--------|
|                                     | a (Å)          | c (Å) | a (Å)            | c (Å)  |
| SnO <sub>2</sub>                    | 4.737          | 3.186 | 4.7460           | 3.1928 |
| SnO <sub>2</sub> + Cu <sup>2+</sup> | 4.737          | 3.186 | 4.7448           | 3.1932 |

In the PXRD pattern of Cu<sup>2+</sup> doped SnO<sub>2</sub> nanoparticles, peaks corresponding to copper was not observed because only a small amount of copper acetate was added as dopant. A slight shift in the diffraction peak towards lower angle was also observed. The broadening of peaks in the pattern indicates the formation of nanostructured material [30]. The average grain size of the particle was calculated using the Scherrer's equation [31].

$$D = \frac{K\lambda}{\beta \cos \theta}$$

where  $\lambda$  is the wavelength of incident beam,  $\beta$  is the full width at half maximum of the diffraction peak (in radian),  $\theta$  is the diffraction angle and  $K$  is the Scherrer's constant (0.9). The average grain size of SnO<sub>2</sub> and Cu<sup>2+</sup> doped SnO<sub>2</sub> nanoparticles are 20.710 nm and 35.960 nm, respectively. The increase in average grain size on the addition of dopant and the shift in peak position towards the lower angle is reported by Haider *et al.* [15].

**Morphological studies:** The morphology and elemental composition of undoped and Cu<sup>2+</sup> doped SnO<sub>2</sub> nanoparticles

were studied using TEM, SEM and EDX analyses. The TEM micrographs and the selective area electron diffraction (SAED) patterns observed are shown in Fig. 3. Particle with spherical morphology and agglomeration was observed in TEM micrographs. Polycrystalline nature of the sample was confirmed by the presence of observable rings in the SAED patterns [32]. The TEM results confirmed that the grain sizes are in nano regime and the inter-planar spacing in the pattern matches well with that in PXRD pattern showing rutile phase of SnO<sub>2</sub>.

The EDX pattern, SEM micrograph along with size distribution are shown in Fig. 4. Agglomeration and spherical morphology was observed in the SEM micrographs. The agglomeration is higher in Cu<sup>2+</sup> doped SnO<sub>2</sub> nanoparticles and it is mainly due to the accumulation of Cu<sup>2+</sup> impurity into host matrix. Spherical morphology along with agglomeration of particles was already reported by several researchers [33-35]. The particle size of SnO<sub>2</sub> and Cu<sup>2+</sup> doped SnO<sub>2</sub> nanoparticles are calculated as 25.5 nm and 37.7 nm.

Occurrence of carbon peaks at 0.27 keV was due to the use of carbon tape substrate for holding the sample while taking the measurement and gold peaks at 2.12 keV was due to the

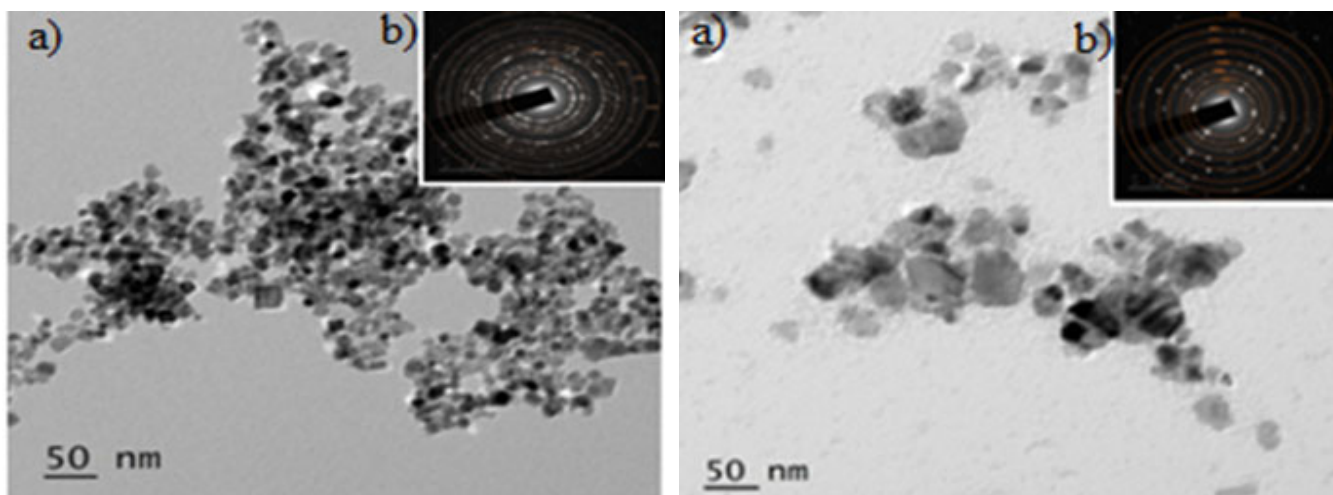


Fig. 3. (a) TEM micrographs and (b) SAED patterns of SnO<sub>2</sub> and Cu<sup>2+</sup> doped SnO<sub>2</sub> nanoparticles

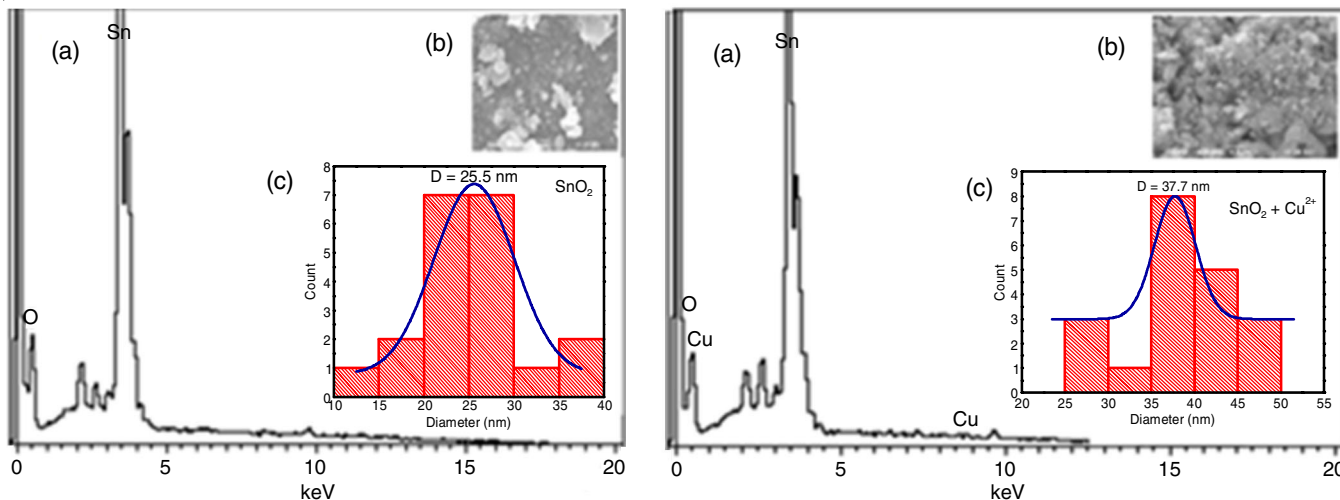


Fig. 4. (a) EDX pattern, (b) SEM micrograph and (c) particle size distribution of SnO<sub>2</sub> and Cu<sup>2+</sup> doped SnO<sub>2</sub> nanoparticles

TABLE-2  
PEAK POSITIONS OF ELEMENTS AND THE ELEMENTAL COMPOSITION OF UNDOPED  
AND Cu<sup>2+</sup> DOPED SnO<sub>2</sub> NANOPARTICLES OBTAINED FROM EDX ANALYSIS

| System (with expected composition)  | Peak positions of elements (keV) |        |        | Elemental composition (atomic %) |        |        |
|-------------------------------------|----------------------------------|--------|--------|----------------------------------|--------|--------|
|                                     | Tin                              | Oxygen | Copper | Tin                              | Oxygen | Copper |
| SnO <sub>2</sub>                    | 3.05                             | 0.52   | –      | 20.32                            | 79.68  | –      |
|                                     | 3.40                             |        |        |                                  |        |        |
|                                     | 3.60                             |        |        |                                  |        |        |
|                                     | 3.90                             |        |        |                                  |        |        |
|                                     | 4.13                             |        |        |                                  |        |        |
| SnO <sub>2</sub> + Cu <sup>2+</sup> | 3.05                             | 0.52   | 0.90   | 20.21                            | 79.57  | 0.22   |
|                                     | 3.40                             |        | 8.00   |                                  |        |        |
|                                     | 3.60                             |        | 8.90   |                                  |        |        |
|                                     | 3.90                             |        |        |                                  |        |        |
|                                     | 4.13                             |        |        |                                  |        |        |

use of gold coating in the sample [36]. The peak positions of elements and the elemental composition of undoped and Cu<sup>2+</sup> doped SnO<sub>2</sub> nanoparticles are shown in Table-2. The EDX results revealed that the prepared samples are free from impurities and hence they have high phase purity.

**UV-Vis NIR studies:** The optical absorption spectra of undoped and Cu<sup>2+</sup> doped SnO<sub>2</sub> nanoparticles are shown in Fig. 5. The spectrum records the variation of optical absorbance with respect to wavelength in the range 200-900 nm. The recorded data can be used to calculate the optical band gap of semiconductor materials or thin films. The prepared sample shows low absorbance in the visible region. In the UV-Vis absorption spectra a sharp increase in absorption was observed at the absorption edge, which corresponds to energies closer to the band gap [37]. The factors influencing the amount of absorption in a material are energy of incoming light, density of electron in valence band and the density of empty states in the conduction band [38]. It was observed that the absorbance decreases with increasing wavelength. Occurrence of absorption peak is mainly due to the excitation of electron from the valence band to the conduction and from this absorption peak the nature and the value of the optical band gap can be determined [39]. In present work, the absorption peak was observed at 278 nm indicating a blue shift as the absorption peak of bulk SnO<sub>2</sub> was 340 nm. Absorption peak at 295 nm and 300 nm

was reported by Rajeswari *et al.* [40] and Alam *et al.* [41] in their work. The optical band gaps of undoped and Cu<sup>2+</sup> doped SnO<sub>2</sub> nanoparticles were calculated using the relation [42]

$$E_g \text{ (eV)} = \frac{hc}{\lambda}$$

where h is the Planck's constant, c is the velocity of light in air and  $\lambda$  is the absorption wavelength in nm. The calculated optical band gaps were 4.474 eV and 4.458 eV.

**Vibrational sample magnetometer analysis:** To study the M-H behaviour of the prepared samples VSM analysis was carried out at room temperature. The diamagnetic nature was observed for undoped and Cu<sup>2+</sup> doped SnO<sub>2</sub> nanoparticles in the M-H curves (Fig. 6). Researchers reported the diamagnetic behaviour of undoped and doped SnO<sub>2</sub> nanoparticles in their studies [43,44]. The structural disorder, electronic structural modifications and surface nature of the nanocrystallites causes diamagnetism in the samples [43].

**Antibacterial activity:** The antibacterial activity was evaluated by measuring the zone of inhibition against the test organisms. The zones of inhibition of undoped and Cu<sup>2+</sup> doped SnO<sub>2</sub> nanoparticles are shown in Table-3. Antibacterial activity of undoped and Cu<sup>2+</sup> doped SnO<sub>2</sub> nanoparticles are shown in Fig. 7. The antibacterial activity occurs due to the formation of reactive oxygen species, large surface area and small particle

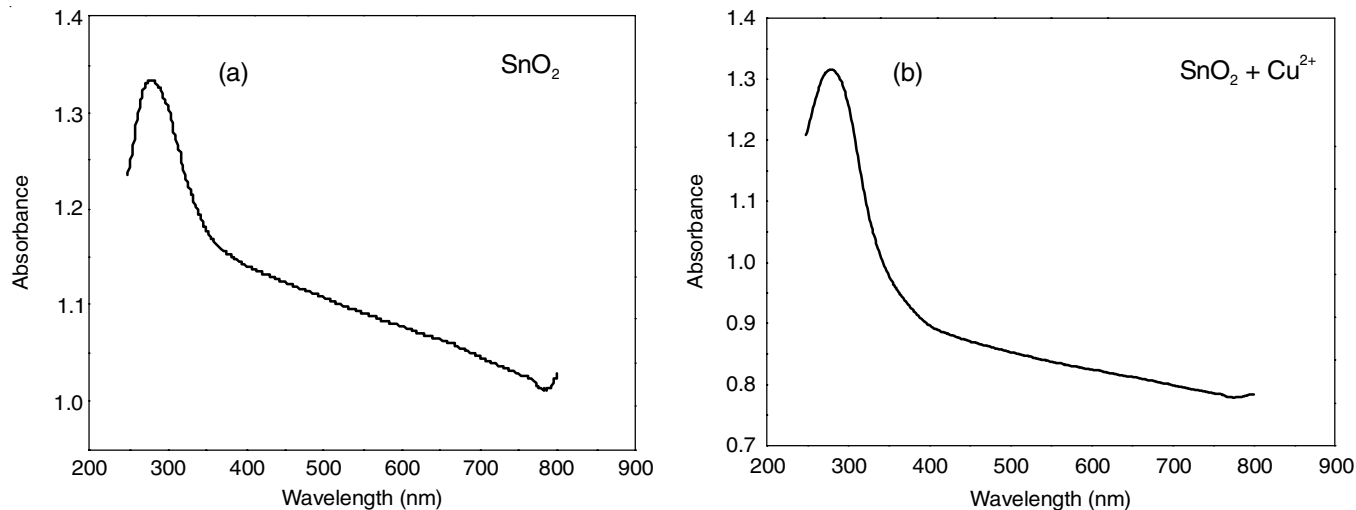


Fig. 5. UV-Vis absorption spectra of (a) SnO<sub>2</sub> and (b) Cu<sup>2+</sup> doped SnO<sub>2</sub> nanoparticles

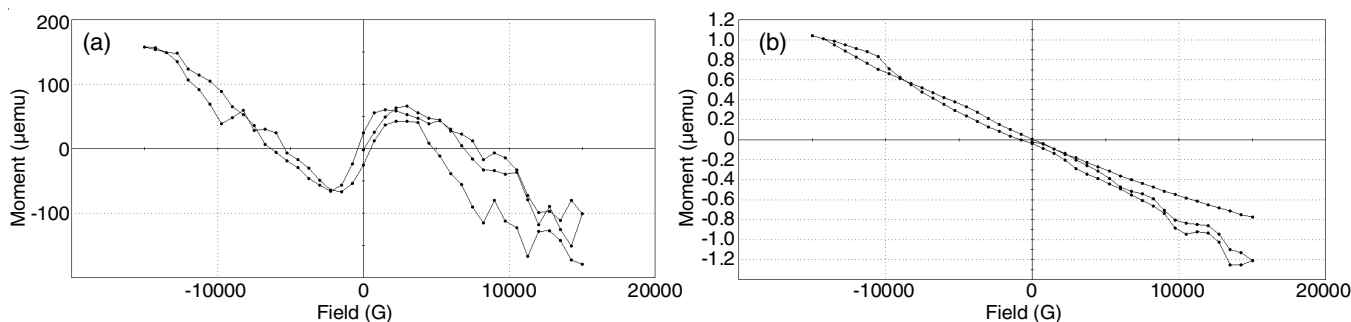


Fig. 6. Magnetization curve of (a) SnO<sub>2</sub> and (b) Cu<sup>2+</sup> doped SnO<sub>2</sub> nanoparticles

TABLE-3  
ZONES OF INHIBITION FOR UNDOPED  
AND Cu<sup>2+</sup> DOPED SnO<sub>2</sub> NANOPARTICLES

| System (with expected composition)  | <i>Staphylococcus aureus</i> | <i>Escherichia coli</i> |
|-------------------------------------|------------------------------|-------------------------|
| SnO <sub>2</sub>                    | 10                           | No zone                 |
| SnO <sub>2</sub> + Cu <sup>2+</sup> | 10                           | 8                       |



Fig. 7. Photograph showing the antibacterial activity of samples against (a) *Staphylococcus aureus* and (b) *Escherichia coli*

size. The reactive oxygen species in particular H<sub>2</sub>O<sub>2</sub> formed on the nanoparticle surface has the ability to penetrate into the cell membrane of bacteria causing damage to the DNA and protein which in turn lead to the death of cells [45-47]. Better activity was observed in Gram positive bacteria than in Gram negative bacteria and it agrees with the results reported by Mirhosseini & Firouzabadi [48] and Azizi *et al.* [49].

## Conclusion

Undoped and Cu<sup>2+</sup> doped SnO<sub>2</sub> nanoparticles were synthesized using a microwave assisted solvothermal method with the help of domestic microwave oven. The prepared samples were annealed at 500 °C for about 1 h. The PXRD pattern shows the tetragonal phase of SnO<sub>2</sub>. The average grain sizes are calculated as 20.710 nm and 35.960 nm. Peak broadening in the pattern indicates the development of nanostructured material. Presence of observable rings in the SAED patterns confirms the polycrystalline nature of the sample. SEM micrographs revealed agglomeration of particles with spherical morphology. The EDX results disclosed the phase purity of the prepared samples. Absorption peak shows the presence of blue shift and it is due to quantum confinement. Vibrational sample magnetometer analysis shows that the prepared samples possess dia-

magnetic behaviour. The antibacterial activities of Cu<sup>2+</sup> doped SnO<sub>2</sub> are competent when compared to undoped sample and hence it can be used in pharmaceutical industries.

## CONFLICT OF INTEREST

The authors declare that there is no conflict of interests regarding the publication of this article.

## REFERENCES

- J. Jeevanandam, A. Barhoum, Y.S. Chan, A. Dufresne and M.K. Danquah, *Beilstein J. Nanotechnol.*, **9**, 1050 (2018); <https://doi.org/10.3762/bjnano.9.98>
- R. Dobrucka and J. Dlugaszewska, *Saudi J. Biol. Sci.*, **23**, 517 (2016); <https://doi.org/10.1016/j.sjbs.2015.05.016>
- H. Li, L. Li and Y. Li, *Nanotechnol. Rev.*, **2**, 515 (2021); <https://doi.org/10.1515/ntrev-2012-0069>
- D.O. Scanlon and G.W. Watson, *J. Mater. Chem.*, **22**, 25236 (2012); <https://doi.org/10.1039/C2JM34352E>
- M. Ghaedi, M. Rahimi, A.M. Ghaedi, I. Tyagi, S. Agarwal and V.K. Gupta, *J. Colloid Interface Sci.*, **461**, 425 (2016); <https://doi.org/10.1016/j.jcis.2015.09.024>
- W. Chen, F. Sun, Z. Zhu, Z. Min and W. Li, *Micropor. Mesopor. Mater.*, **186**, 65 (2014); <https://doi.org/10.1016/j.micromeso.2013.11.030>
- F. Shao, F. Hernandez-Ramirez, J.D. Prades, J.R. Morante and N. Lopez, *Procedia Eng.*, **47**, 293 (2012); <https://doi.org/10.1016/j.proeng.2012.09.141>
- D. Singh, V.S. Kundu and A.S. Maan, *J. Mol. Struct.*, **1100**, 562 (2015); <https://doi.org/10.1016/j.molstruc.2015.08.009>
- B. Lee, S.C. Han, M. Oh, M.S. Lah, K.-S. Sohn and M. Pyo, *Electrochim. Acta*, **113**, 149 (2013); <https://doi.org/10.1016/j.electacta.2013.09.093>
- F. Prado, H.F. Andersen, M. Taeño, J.P. Mæhlen, J. Ramírez-Castellanos, D. Maestre, S. Karazhanov and A. Cremades, *Sci. Rep.*, **10**, 5503 (2020); <https://doi.org/10.1038/s41598-020-62505-x>
- M.A. Batal and F.H. Jneed, *Energy Procedia*, **6**, 1 (2011); <https://doi.org/10.1016/j.egypro.2011.05.001>
- X. Qiao, H. Yang, C. Chen, X. Lou, J. Sun, L. Chen, X. Fan, L. Zhang and Q. Shen, *Procedia Eng.*, **94**, 58 (2014); <https://doi.org/10.1016/j.proeng.2013.11.044>
- R. Udayakumar, V. Khanaaand and T. Saravanan, *Indian J. Sci. Technol.*, **6**, 4754 (2013).
- M.A.M. Akhir, K. Mohamed, H.L. Lee and S.A. Rezan, *Procedia Chem.*, **19**, 993 (2016); <https://doi.org/10.1016/j.proche.2016.03.148>
- A.J. Haider, S.S. Shaker and A.H. Mohammed, *Energy Procedia*, **36**, 776 (2013); <https://doi.org/10.1016/j.egypro.2013.07.090>
- H. Taib and C.C. Sorrell, *J. Aust. Ceram. Soc.*, **43**, 56 (2007).
- S. Sagadevan, *J. Nanomater. Mol. Nanotechnol.*, **4**, 4 (2015); <https://doi.org/10.4172/2324-8777.1000157>

18. T. Krishnakumar, N. Pinna, K.P. Kumari, K. Perumal and R. Jayaprakash, *Mater. Lett.*, **62**, 3437 (2008);  
<https://doi.org/10.1016/j.matlet.2008.02.062>
19. L. Zhang, J. Wu, F. Chen, X. Li, J.M. Schoenung and Q. Shen, *J. Asian Ceramic Soc.*, **1**, 114 (2013);  
<https://doi.org/10.1016/j.jascer.2013.03.010>
20. N.S. Sabri, M.S.M. Deni, A. Zakaria and M.K. Talari, *Phys. Procedia*, **25**, 233 (2012);  
<https://doi.org/10.1016/j.phpro.2012.03.077>
21. J. You, Y. Zhang and Z. Hu, *Colloids Surf. B Biointerfaces*, **85**, 161 (2011);  
<https://doi.org/10.1016/j.colsurfb.2011.02.023>
22. A.S.H. Hameed, C. Karthikeyan, A.P. Ahamed, N. Thajuddin, N.S. Alharbi, S.A. Alharbi and G. Ravi, *Sci. Rep.*, **6**, 24312 (2016);  
<https://doi.org/10.1038/srep24312>
23. S. Haq, W. Rehman, M. Waseem, A. Shah, A.R. Khan, M.U. Rehman, P. Ahmad, B. Khan and G. Ali, *Mater. Res. Express*, **7**, 025012 (2020);  
<https://doi.org/10.1088/2053-1591/ab6fa1>
24. J.E. Jeronsia, L.A. Joseph, M.M. Jaculine, P.A. Vinosha and S.J. Das, *J. Taibah Univ. Sci.*, **10**, 601 (2016);  
<https://doi.org/10.1016/j.jtusc.2015.12.003>
25. S.M. Amininezhad, A. Rezvani, M. Amouheidari, S.M. Amininejad and S. Rakhshani, *Zahedan J. Res. Med. Sci.*, **17**, e1053 (2015);  
<https://doi.org/10.17795/zjrms-1053>
26. G.R. Navale, M. Thripuranthaka, D.J. Late and S.S. Shinde, *JSM Nanotechnol. Nanomed.*, **3**, 1033 (2015).
27. A. Azam, A.S. Ahmed, M. Oves, M.S. Khan, S.S. Habib and A. Memic, *Int. J. Nanomedicine*, **7**, 6003 (2012);  
<https://doi.org/10.2147/IJN.S35347>
28. N. Yongvanich, P. Visuttipitukkul, W. Assawasilapakul, W. Srichan and S. Onlamoon, *Energy Procedia*, **9**, 498 (2011);  
<https://doi.org/10.1016/j.egypro.2011.09.057>
29. F. Yang, X. Zhang, F. Tian, X. Wu and F. Gan, *Chin. J. Aeronaut.*, **20**, 181 (2007);  
[https://doi.org/10.1016/S1000-9361\(07\)60030-2](https://doi.org/10.1016/S1000-9361(07)60030-2)
30. A. Ramazani, S. Hamidi and A. Morsali, *J. Mol. Liq.*, **157**, 73 (2010);  
<https://doi.org/10.1016/j.molliq.2010.08.012>
31. P.K. Baitha, P.P. Pal and J. Manam, *Nucl. Instrum. Methods Phys. Res. A*, **745**, 91 (2014);  
<https://doi.org/10.1016/j.nima.2014.01.041>
32. K.-M. Lee, D.-J. Lee and H. Ahn, *Mater. Lett.*, **58**, 3122 (2004);  
<https://doi.org/10.1016/j.matlet.2004.06.002>
33. S. Tazikeh, A. Akbari, A. Talebi and E. Talebi, *Mater. Sci. Pol.*, **32**, 98 (2014);  
<https://doi.org/10.2478/s13536-013-0164-y>
34. S.M. Priya, A. Geetha and K. Ramamurthi, *J. Sol-Gel Sci. Technol.*, **78**, 365 (2016);  
<https://doi.org/10.1007/s10971-016-3966-7>
35. J. Gajendiran and V. Rajendran, *Optoelectron. Adv. Mater. Rapid Commun.*, **5**, 44 (2011).
36. S. Kumar, R. Nigam, V. Kundu and N. Jaggi, *J. Mater. Sci. Mater. Electron.*, **26**, 3268 (2015);  
<https://doi.org/10.1007/s10854-015-2826-5>
37. J.C.V. Manikandan, M. Singh, B.C. Yadav, R.S. Mane and S. Vigneselvan, *Mater. Chem. Phys.*, **240**, 122265 (2020);  
<https://doi.org/10.1016/j.matchemphys.2019.122265>
38. T.J. Jacobsson, Ph.D. Thesis in Materials Chemistry, Synthesis and Characterization of ZnO Nanoparticles, Uppsala Universitet, Sweden (2009).
39. S. Kar and S. Kundoo, *Int. J. Sci. Res.*, **4**, 530 (2015).
40. S. Rajeswari, J. Uma Maheswari, D. Muthuraj, E. Kumar and V. Veeraputhiran, *J. Nanosci. Tech.*, **5**, 637 (2019);  
<https://doi.org/10.30799/jnst.214.19050115>
41. M. Alam, A.A. Ansari, M.R. Shaik and N.M. Alandis, *Arab. J. Chem.*, **6**, 341 (2013);  
<https://doi.org/10.1016/j.arabjc.2012.04.021>
42. K.U. Madhu, Ph.D. Thesis, Studies of ZnO-CdS Nanocomposites, Manonmaniam Sundaranar University, Abishekapatti, India (2010).
43. K. Sakthiraj, B. Karthikeyan and K. Balachandrakumar, *Int. J. Chemtech Res.*, **7**, 1481 (2015).
44. S.H. Babu, N.M. Rao, S. Kaleemulla, G. Amarendra and C. Krishnamoorthi, *Bull. Mater. Sci.*, **40**, 17 (2017);  
<https://doi.org/10.1007/s12034-016-1352-2>
45. D. Chandran, L.S. Nair, S. Balachandran, K.R. Babu and M. Deepa, *J. Sol-Gel Sci. Technol.*, **76**, 582 (2015);  
<https://doi.org/10.1007/s10971-015-3808-z>
46. K.R. Raghupathi, R.T. Koodali and A.C. Manna, *Langmuir*, **27**, 4020 (2011);  
<https://doi.org/10.1021/la104825u>
47. Y. Xie, Y. He, P.L. Irwin, T. Jin and X. Shi, *Appl. Environ. Microbiol.*, **77**, 2325 (2011);  
<https://doi.org/10.1128/AEM.02149-10>
48. M. Mirhosseini and F.B. Firouzabadi, *Int. J. Dairy Technol.*, **66**, 291 (2013);  
<https://doi.org/10.1111/1471-0307.12015>
49. S. Azizi, M.B. Ahmad, F. Namvar and R. Mohamad, *Mater. Lett.*, **116**, 275 (2014);  
<https://doi.org/10.1016/j.matlet.2013.11.038>